

# CONTINUOUS FIBER ANGLE TOPOLOGY OPTIMIZATION FOR POLYMER FUSED FILAMENT FABRICATION

R. Hoglund and D.E. Smith

Department of Mechanical Engineering, Baylor University, Waco, TX 76798

## Abstract

Mechanical properties of parts produced with the Fused Filament Fabrication (FFF) process are known to be dependent on the printed bead direction, especially when short carbon fiber reinforcement is added to the filament. Given that many FFF filament suppliers now offer carbon-fiber filled products, a unique opportunity emerges in the design of polymer composite FFF parts since bead and fiber direction can potentially be prescribed to give the best structural performance. As FFF moves from a technology for rapid prototyping and the hobbyist to a viable additive manufacturing method, it is important to also have a design tool that takes advantage of the opportunities that present themselves when polymer composites are employed. This paper presents a topology optimization method for continuous fiber angle optimization approach (CFAO), which computes optimal material distribution (as in the well known SIMP method) in addition to a preferred fiber angle direction by minimizing compliance of statically loaded structures. Our computed results show the effects of variable orientation angle on fiber reinforced microstructure for the topology of two-dimensional FFF parts. Optimal fiber orientations are shown to align with the axis of structural members that form within the structure as expected. Example design problems are solved and then printed on desktop 3D FFF printers using the material distribution results and a simple infill method which approximates the optimal fiber angle results by a contour-parallel deposition strategy. Mechanical stiffness testing of the printed parts show improved results as compared to structures designed without accounting for the direction of the composite structure. Future work includes extension of the method to three dimensional structures for further application.

## Introduction

The use of Fused Filament Fabrication (FFF) has expanded greatly over the past two decades due in part to its low cost and selection of materials. Unfortunately, the reduced mechanical properties of a typical FFF layered structure must be addressed for this technology to reach its full potential in producing engineering products. The method of extrusion during part processing has been shown to give the final FFF product non-isotropic properties with increased stiffness in the deposition direction [1]. The stiffness and strength of ABS polymer structures produced with FFF has also been shown to improve with the added reinforcement of single-walled carbon nanotubes and short glass fibers [2], [3]. Recently, the effects of carbon fiber content and fiber length have been found to increase the Young's modulus of FFF parts to varying degrees [4], increasing the modulus of elasticity by as much as 4X in the print direction.

Topology optimization has been shown to be an effective tool for the design of structures produced with additive manufacturing where an optimal material distribution in a design domain is determined for a given material volume [5], [6]. Topology optimization is commonly performed to maximize the stiffness of a part while retaining a given fraction of material volume

in the design domain. The Homogenization Method was developed to determine an optimal material distribution and orthotropic material orientation distribution within a structure [7]. Unfortunately, the homogenization method, as well as SIMP methods that have been extended to include pointwise material orientation as part of the design problem [8], is impractical to implement in FFF, as it is not possible to produce a part where each point within the structure has a unique material direction and/or continuously varying density. An alternative approach, the SIMP (Solid Isotropic Material with Penalization) method [9], or density method [10], computes material distributions for isotropic materials. The SIMP method has seen extensive use in additive manufacturing where unique three dimensional microstructures designed for a prescribed mechanical response are printed with additive manufacturing methods (see e.g., Hollister, et al. [11]). More recently, the distribution of varying microstructure has been computed with a modified SIMP method where the printed optimal design includes the details of optimal unit cell geometries (see e.g., Sundararajan (2010) and Zhang, et al. [12]), [13]. This later research computes the effective orthotropic material matrix for a unit cell having varying density which serves as the design variable in the topology optimization. Alamo and da Silva extended the SIMP method to compute a material distribution for a fixed orthotropic material distribution in a biomechanics structure [14].

Unfortunately, none of these methods have addressed the need for having discrete material distributions (such as those computed with SIMP methods (see e.g., [15,16,18]) and also a preferred fiber direction that are suitable for parts produced with the FFF process. This paper builds on our earlier work of topology optimization with a fixed fiber angle [20,21]. Here we consider a modified SIMP approach which we call the Continuous Fiber Angle Optimization (CFAO) method that determines the optimal distribution of an orthotropic material and its orthotropic material orientation to design fiber-reinforced FFF parts. This paper also includes a methodology for printing FFF parts that have the optimal topology and fiber angle, and provides experimental results to verify the usefulness of our CFAO approach.

### **Two-Dimensional Continuous Fiber Angle Optimization**

A Continuous Fiber Angle Optimization (CFAO) method is introduced here that is used to compute the optimal topology and fiber angle of planar FFF structures that are produced with an orthotropic microstructure. In the topology optimization problem, each element is assigned an independent elemental density  $\rho_e$  and element fiber angle  $\theta_e$ , which collectively compose the design variable vector in the optimization problem. Our finite element-based approach is derived from the density or SIMP method [9] where each elemental density  $\rho_e$  (assembled in a density array  $\boldsymbol{\rho}$ ) is used to scale its respective element stiffness matrix  $\mathbf{k}_e$  within the design domain of the finite element model. In CFAO, the element fiber angle  $\theta_e$  (assembled in a fiber angle array  $\boldsymbol{\theta}$ ) is introduced to define the direction of orthotropy. The topology optimization problem that minimizes the compliance  $c$  subject to a constraint on volume fraction  $f$  is stated in the usual manner as [9,15]

$$\text{Minimize: } c(\boldsymbol{\rho}, \boldsymbol{\theta}) = \mathbf{U}^T \mathbf{F} = \mathbf{U}^T \mathbf{K} \mathbf{U} = \sum_{e=1}^N (\rho_e)^p \mathbf{u}_e^T \mathbf{k}_e(\theta_e) \mathbf{u}_e \quad (1)$$

$$\text{Subject to: } \frac{V(\boldsymbol{\rho})}{V_0} \leq f, \mathbf{K} \mathbf{U} = \mathbf{F}, \rho_{min} \leq \rho_e \leq 1, -2\pi \leq \theta_e \leq 2\pi \quad (2)$$

where the volume  $V(\boldsymbol{\rho})$  of material in the optimal design is limited to  $f V_0$  where  $V_0$  is the total volume of the design space as is typical in topology optimization. The equilibrium equations for the structure are solved with the finite element method as  $\mathbf{K}\mathbf{U} = \mathbf{F}$  where  $\mathbf{K}$ ,  $\mathbf{U}$ , and  $\mathbf{F}$  are the global stiffness matrix, displacement vector, and applied load vector, respectively. In the above, the compliance is defined as the product  $\mathbf{U}$  and  $\mathbf{F}$ , and may be computed at the element level in terms of the element density  $\rho_e$ , displacement vector  $\mathbf{u}_e$  and stiffness matrix  $\mathbf{k}_e$  as shown.

Note that each  $\mathbf{k}_e$  is multiplied by its element density  $\rho_e$  which is raised to the power  $p$  which is identified as the penalization parameter [9]. The penalization parameter  $p$  is fixed with respect to design and causes each  $\rho_e$  to move toward either its lower or upper bound, i.e.,  $\rho_{min}$  or 1, respectively, in the optimization. The element fiber angle array  $\boldsymbol{\theta}$  (with each element fiber angle  $\theta_e$  being constrained between  $\pm 2\pi$  in Equ. 2) enters the topology optimization problem through the element stiffness matrices given as

$$\mathbf{k}_e(\theta_e) = \iint_{\Omega_e} h \mathbf{B}^T \mathbf{C}'(\theta_e) \mathbf{B} d\Omega \quad (3)$$

where 2D integration is performed over each element domain  $\Omega_e$  and  $h$  is the element thickness normal to the plane of the structure. The finite element strain-displacement matrix  $\mathbf{B}$  is defined in the usual manner in terms of the element shape functions. Note that we use an isoparametric mapping and Gauss quadrature (not shown) to numerically compute the element stiffness matrices as is typical in finite element analyses. The fiber angle design variables  $\theta_e$  enter the optimization problem through the rotated elastic constitutive matrix  $\mathbf{C}'(\theta_e)$  defined as

$$\mathbf{C}'(\theta_e) = \mathbf{T}(\theta_e)^{-1} \mathbf{C} \mathbf{T}(\theta_e)^{-T} \quad (4)$$

where

$$\mathbf{T}^{-1}(\theta_e) = \begin{bmatrix} \cos^2\theta_e & \sin^2\theta_e & -2\cos\theta_e\sin\theta_e \\ \sin^2\theta_e & \cos^2\theta_e & 2\cos\theta_e\sin\theta_e \\ \cos\theta_e\sin\theta_e & -\cos\theta_e\sin\theta_e & \cos^2\theta_e - \sin^2\theta_e \end{bmatrix} \quad (5)$$

is the inverse of the transformation matrix  $\mathbf{T}$  used to rotate the elastic two-dimensional orthotropic constitutive matrix  $\mathbf{C}$  given as

$$\mathbf{C} = \begin{bmatrix} \frac{E_1}{1-\nu_{12}\nu_{21}} & \frac{\nu_{21}E_1}{1-\nu_{12}\nu_{21}} & 0 \\ \frac{\nu_{21}E_1}{1-\nu_{12}\nu_{21}} & \frac{E_2}{1-\nu_{12}\nu_{21}} & 0 \\ 0 & 0 & G_{12} \end{bmatrix} \quad (6)$$

The constitutive matrix  $\mathbf{C}$  is defined in Equ. 6 in terms of the principal moduli of elasticity  $E_1$  and  $E_2$ , and Poisson's ratios  $\nu_{12}$  and  $\nu_{21}$ , which are related through

$$\frac{E_1}{\nu_{21}} = \frac{E_2}{\nu_{12}} \quad (7)$$

In the optimization examples below, we define  $E_1 = \alpha E_2$ , where  $1 \leq \alpha \leq 10$  is employed. It follows that  $\nu_{21} = \alpha \nu_{12}$ . The influence of  $\alpha$  on shear modulus is approximated in our work though  $G_{12} = \frac{E_1}{2(1+\nu_{12})}$ .

Due to the large number of design variables, the CFAO approach employs the Adjoint Variable Method (see e.g., [10]) to compute the design sensitivities of the compliance with respect to the density and fiber angle design variables. It is easy to show that for compliance, the adjoint variable vector is the displacement vector  $\mathbf{U}$ , making it possible to write components of the compliance gradient in terms of element density  $\rho_e$  as

$$\frac{\partial c}{\partial \rho_e} = -p \rho_e^{p-1} \mathbf{u}_e^T \mathbf{k}_e \mathbf{u}_e \quad (8)$$

which is obtained by taking the derivative of  $c$  in Equ. 1 with respect to density  $\rho_e$ . In addition, derivatives of  $c$  with respect to fiber angle  $\theta_e$  are obtained from Eqs. 1, 3-5 as

$$\frac{\partial c}{\partial \theta_e} = -\rho_e^p \mathbf{u}_e^T \left\{ \iint_{\Omega_e} h \left( \mathbf{B}^T \frac{\partial \mathbf{T}^{-1}}{\partial \theta_e} \mathbf{C} \mathbf{T}^{-T} \mathbf{B} + \mathbf{B}^T \mathbf{T}^{-1} \mathbf{C} \frac{\partial \mathbf{T}^{-T}}{\partial \theta_e} \mathbf{B} \right) d\Omega \right\} \mathbf{u}_e \quad (9)$$

Derivatives of  $\mathbf{T}^{-1}$  in Equ. 5 with respect to  $\theta_e$  follow in the usual manner. Note that since each element density design variable  $\rho_e$  and each element fiber angle  $\theta_e$  are associated with a single element, the derivatives in Eqs. 8 and 9 yield only the single term from the element sum in Equ. 1 as shown.

To eliminate checkerboarding, we employ the mesh independent sensitivity filter used in Sigmund [14,16] given as

$$\widetilde{\frac{\partial c}{\partial \rho_e}} = \frac{\sum_{i=1}^{N_e} w(x_i) \rho_i}{\rho_e \sum_{i=1}^{N_e} w(x_i)} \frac{\partial c}{\partial \rho_e} \quad (10)$$

where  $w(x_i)$  is a weighting function that places more emphasis on elements that are close to the element of interest based on the radial distance  $x_i$ . Our results have shown that this filter alone eliminates checkerboarding without the need for also including a filter on either the  $\rho_e$  or  $\theta_e$ .

Our CFAO method is implemented using a custom 2D plane stress finite element program and the `fmincon` function of Matlab (The Mathworks, Inc., Natick, MA). Isoparametric finite elements are used and the program also computes the design sensitivities from Eqs. 8-10 once the finite element solution  $\mathbf{U}$  is known. The user defined gradient option of `fmincon` is employed for the compliance objective function, and the volume constraint is implemented using the linear inequality constraint feature. The interior-point optimization algorithm in `fmincon` was used since it accepts gradients and was found to work well with our large scale optimizations. In the following examples,  $f = 0.5$ , and  $p = 3$ , and the initial design was specified as  $\rho_e = 0$  for all density variables and  $\theta_e = 0$  for all fiber angle design variables. The accuracy of the design sensitivities computed with Eqs. 8 and 9 was verified with finite difference derivative computations using the forward finite difference method prior to running the topology optimizations that appear below.

## CFAO Computational Results

In order to illustrate the applicability of the orthotropic model to polymer composite FFF part design, several topology optimization of a 2D model are considered based on the Messerschmitt-Bölkow-Blohm (MBB) beam [17]. The MBB beam is a truss-like structure popularized in many topology optimization studies. Here we first consider the topology optimization of a half-symmetry model of the MBB beam appearing in Figure 1, and then solve the optimization problem for the complete domain in Figure 3. In all cases, the lesser Young's modulus is set to 1 while the modulus ratio  $a$  ranges from 1 to 10. Poisson's ratio of the major direction (greater Young's modulus) is defined to be 0.36, an approximate ratio for polylactic acid (PLA) polymer-printed structures, and  $p = 3$ . The topology optimization scheme iterates until the greatest change in elemental density is less than 1%. In the following, all elements contain a density and fiber angle design variable which produces a topology optimization problem from Eqs. 1 and 2 where the number of design variables equates to two times the number of elements. The thickness of the model into the plane is  $h = 1$ .

We first consider the simple cantilever beam design shown in Fig. 1 to illustrate our CFAO topology optimization process. The beam finite element model has 30 elements in the horizontal direction and 10 elements in the vertical direction. The elastic constants are  $E_1 = 5$  and  $E_2 = 1$ , and  $\nu_{12} = 0.3$ , making  $\alpha = 5$ . The applied load is 1 and acts downward on the right lower edge of the design domain.



Figure 1: Cantilever beam example showing loading and boundary conditions.

Selected designs taken from iterations of the CFAO topology optimization appear in Fig. 2. Elements in the figure appear dark as  $\rho_e$  approaches unity (i.e., element full of material), and white as  $\rho_e$  approaches zero (i.e., no material). Also shown in each element is an arrow indicating the fiber angle direction. Note that all  $\theta_e$  are zero for the initial design and quickly change to become parallel to the direction of the dominant structure in the truss-like members. The topology of the structure emerges after just 25 iterations, however, the edge of the truss-like becomes more distinct as the optimization concludes. We found that the minimum compliance indicated a much stiffer structure when compared to our earlier results that only considered a variable element density while fixing the fiber angle in either the 1- or 2-direction.

We next consider the MBB beam design space appearing in Fig. 3. The design domain has a base width of 120 and a height of 20, yielding 2400 elements and 4800 design variables in the CFAO optimizations. Material properties and optimization initial conditions are the same as those given above for the cantilever beam. The load is 1 unit in the negative  $x_2$  direction applied

at the midpoint of the top of the beam. Optimal topologies for varies values of  $\alpha$  ranging from 1.33 to 10 appear in Fig. 4. Notice that little change in topology is seen for  $\alpha > 1.33$  indicating that the modulus ratio has little effect on topology when fiber angle is included as a design variable in the optimization.

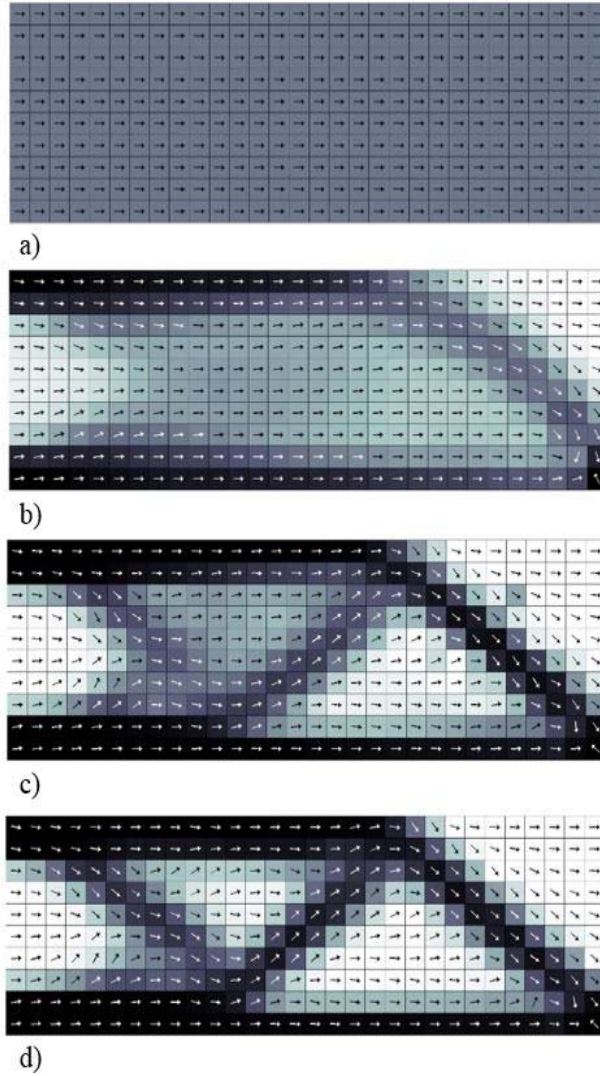


Figure 2: CFAO results for a cantilever beam after a) 0 iterations (i.e., initial design), b) 5 iterations, c) 25 iterations, and d) final iteration 48.

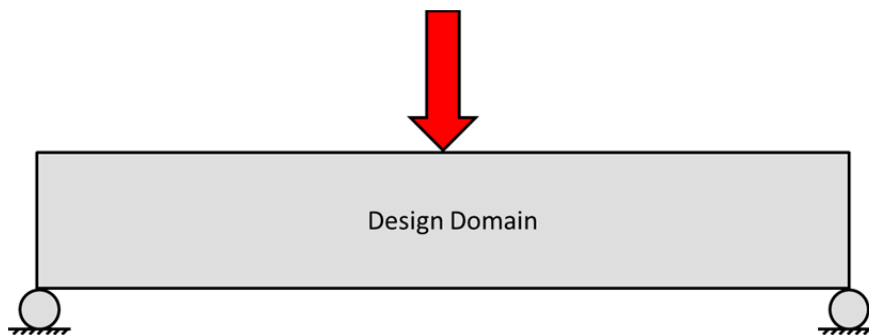


Figure 3: MBB beam design space with boundary conditions and applied load.

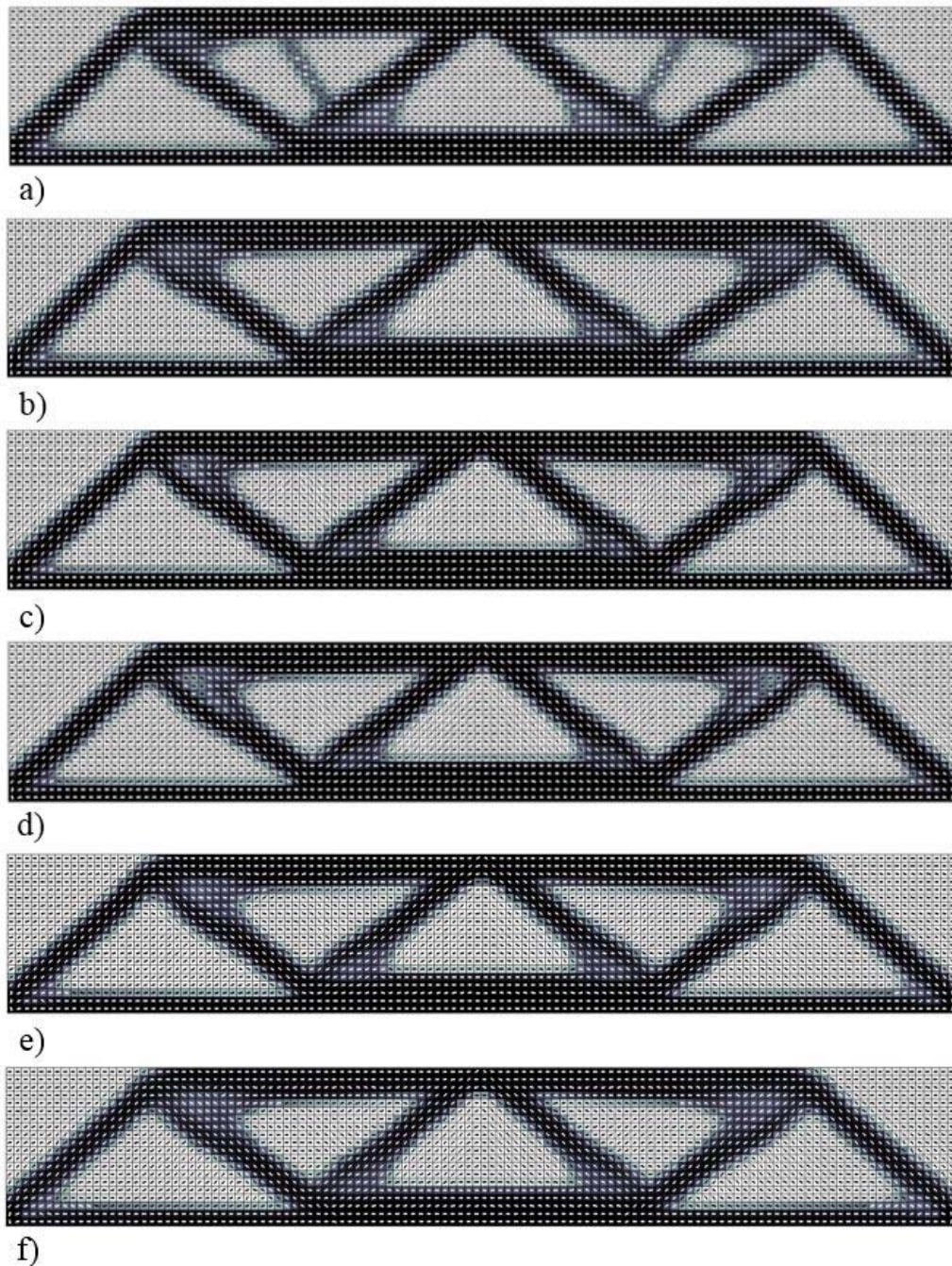


Figure 4: CFAO optimization results for the MBB beam with varying  $\alpha$ . a)  $\alpha = 1.33$ , b)  $\alpha = 1.5$ , c)  $\alpha = 2$ , d)  $\alpha = 5$ , and e)  $\alpha = 10$ .

Values of optimal compliance, CPU time, and number of optimization iteration are given in Table 1. It is shown that the optimal compliance decreases considerable, however, this value alone is not a good comparative measure between these designs since the overall stiffness of the material increases with  $\alpha$  since  $E_2 = 1$  for all optimizations. It is interesting that as  $\alpha$  increases, the number of optimization iterations do so also, as does the CPU time (CPU time reported for an Intel i7-4930K CPU at 3.4 GHz and 64 GB RAM). CPU times for the CFAO optimizations

where found to be significantly higher than our earlier fixed fiber angle optimizations as described in Hoglund [21]. This is due, in part, to the use of different optimization algorithms for the CFAO and fixed angle optimizations which employed the optimality criteria method given in Sigmund [15].

Upon comparing these results to our earlier work with fixed horizontal fiber angle (i.e., all  $\theta_e = 0$ ) [20,21], we find that a lower minimum compliance is obtained for all  $\alpha > 2$  using the CFAO method. Optimization problems are inherently nonlinear, which can result in convergence to various local minimum points. Our results tended to converge to topologies typical of earlier MBB beam optimization, mitigating our concern that local minimum is an issue. Future work should include additional computations to ensure that solutions obtained here are indeed the global minimum.

| <b>Modulus ratio <math>\alpha</math></b> | <b>Number of Iterations</b> | <b>CPU Time (sec)</b> | <b>Minimum Compliance</b> |
|--|-----------------------------|-----------------------|---------------------------|
| 1.33                                     | 44                          | 586                   | 86.21                     |
| 1.5                                      | 62                          | 911                   | 70.39                     |
| 2  | 72                          | 994                   | 53.59                     |
| 5  | 180                         | 2379                  | 22.54                     |
| 10                                       | 169                         | 2224                  | 12.06                     |

Table 1: CFAO MBB optimization results for various modulus ratio  $\alpha$ .

### **Fabrication and Testing of Optimal CFAO Designs**

In order to further demonstrate the usefulness of the CFAO method, optimized MBB beams are printed with varying orientations using carbon fiber-reinforced PLA sold as 3DXMax CFR-PLA by 3DxTECH (3DXTECH, Byron Center, MI). The filament contains approximately 15% carbon fibers by weight in a 1.77 mm diameter filament and has a published tensile strength of 47.9 MPa and a tensile modulus of 4.791 GPa. For FFF processing, our MBB structures are printed with a MakerBot Replicator 2.0 3D FFF printer with a hardened steel 0.6 mm diameter nozzle. The geometry of the printed MBB beams was taken from the optimized result for  $\alpha = 10$  that appears in Fig. 4f. Our FFF structures are printed with 100% infill to reduce interbead voids within the material, and are printed with a thickness of 5.5 mm and a layer thickness of 0.2 mm. The CFAO MBB beam selected for printing is shown in Fig. 5a which was computed with 180 elements in the horizontal direction and 30 elements in the vertical direction (resulting in 5400 elements and 10,800 design variables).

To produce a printable format of the topology optimizations, the code `Top3dSTL_v3.m` was used to convert the physical array of elemental densities to .stl file format [19]. We use `Top3dSTL_v3.m` to translate the optimal density distributions to an STL where each element represents a unit cube. The 2-dimensional information for the planar MBB beams is retained while the thickness out-of-plane is modified to adjust for scaling of the part dimensions in the plane. Autodesk MeshMixer (AutoDesk, San Rafael, CA) is used to smooth the edges of the CFAO structures prior to printing. This smoothing helps to facilitate a printed part that has beads



with a primary orientation that is parallel to the edge of the truss-like members that result from the CFAO optimizations. To realize print paths that remain mostly parallel to the edge of the structure, a contour-parallel deposition strategy is employed. In this case, the strategy is implemented by specifying a high number of shell layers in the MakerBot Desktop software to ensure so that all printed beads approximately align with the edges, particularly within the structural members that form. Fig. 5 shows the model data (left half of beam only) at various stages during the processing of data for printing which includes the CFAO optimized topology and fiber angle, the smoothed image obtained with Autodesk MeshMixer, and the bead pattern print path as specified by the MakerBot Desktop. The resulting printed beam appears in Fig. 6.

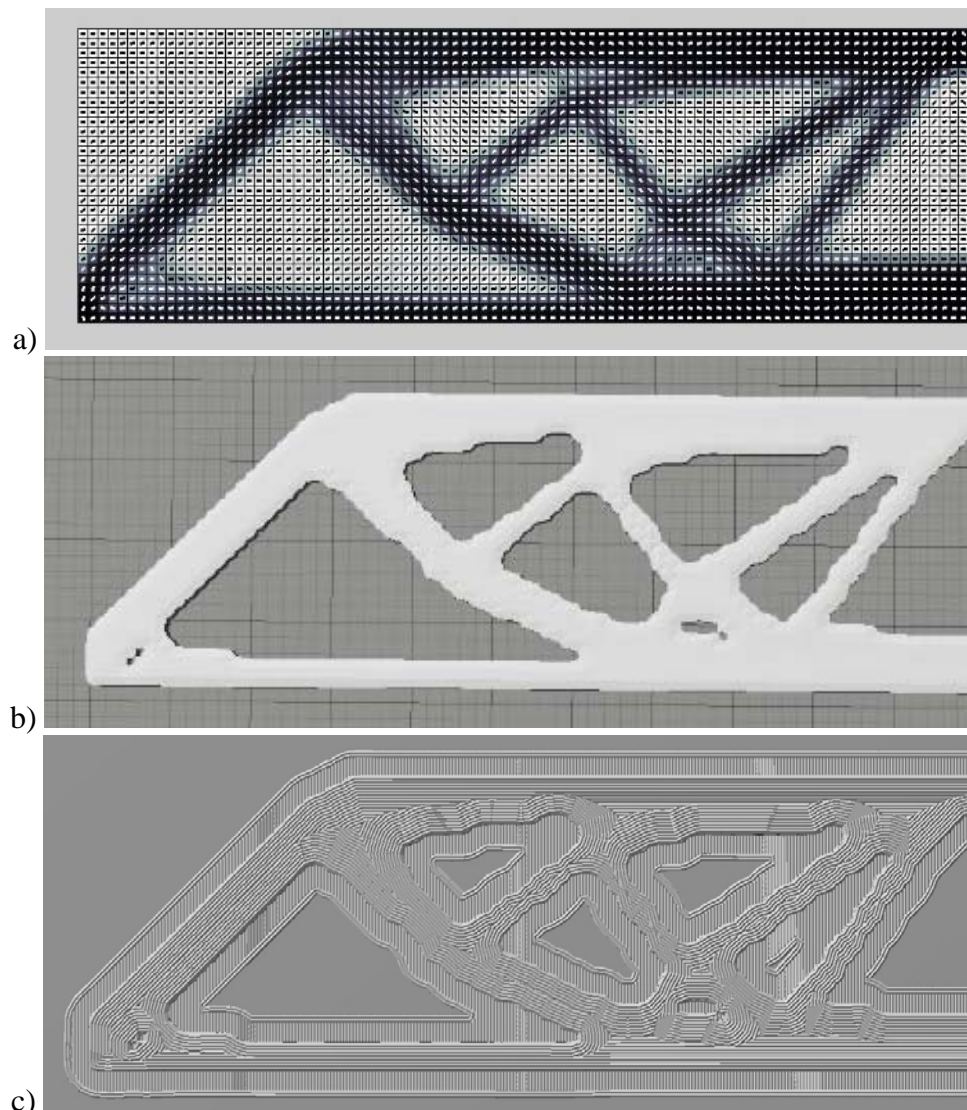


Figure 5: CFAO optimized MBB print data (left half only) of a) optimized density and fiber angle distribution (5400 element model), b) MeshMixer smoothed STL file data, and c) MakerBot Desktop print bead pattern.

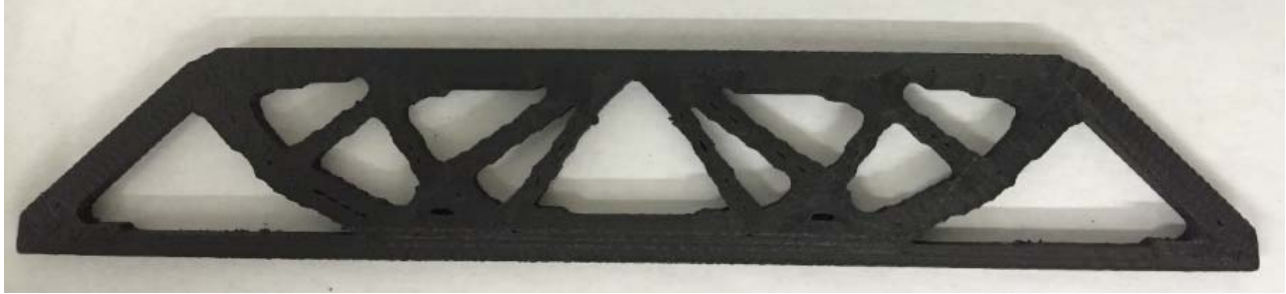


Figure 6: Printed CFAO optimized MBB beam.

Printed CFAO optimized MBB beams were tested in 3-point bending as shown in Fig. 7 using an Instron (Instron, Norwood, MA) tensile test machine with a 2kN load cell. The load is applied to the top center of the printed beam in the same manner as that used in the CFAO optimization. The structural stiffness was computed from force and displacement data that was collected using the Bluehill 3 (Instron, Norwood, MA) software. Loading was performed in the linear force-displacement range for the sample and testing was ended prior to sample failure.

Three samples were printed and tested to obtain the stiffness results given in Table 2. Also shown in Table 2 are results from similar tests (3 samples each) where optimal topologies were computed assuming a fixed horizontal bead path (i.e.,  $\theta_e = 0$ ) and a fixed vertical bead path (i.e.,  $\theta_e = 90^\circ$ ) as described in [20,21]. Note that in these structures with a fixed fiber angle, each element has a single density design variable, which simplify the calculations and the process for creating the print file. The fixed angle optimizations provide a point of comparison to illustrate the effectiveness of the CFAO method. As shown in Table 2, samples optimized and printed with a horizontal bead are 15.5% stiffer than samples optimized and printed with a predominant vertical bead. This result is to be expected since horizontal stiffening is more efficient than vertical stiffening under the given bending load. Table 2 also shows that CFAO optimized MBB beams perform better than either horizontal or vertical optimized and printed beams. It is seen that the CFAO beam is 29.9% stiffer than the vertical optimized and printed structure and 12.4% stiffer than the horizontal optimized and printed structure.

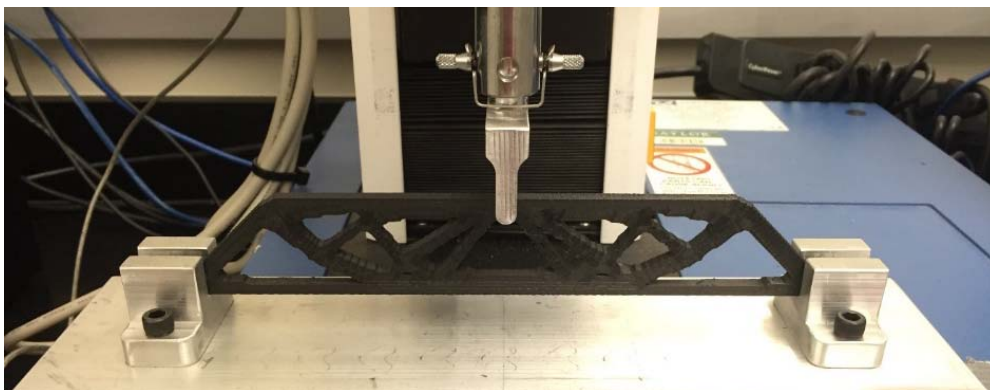


Figure 7: Mechanical test set up for CFAO optimized MBB beam.

More information on details of the optimization and testing may be found in Hoglund [20,21] which also includes the CFAO optimization and testing of the Mitchell truss [17].

## Conclusions and Future Work

The CFAO method for topology optimization of 2D anisotropic structures has been developed which includes both material distribution and angle of preferred modulus, where special consideration is given to carbon fiber-reinforced Fused Filament Fabrication products. The stiffness of the structures are maximized for a given volume fraction by determining the optimal element densities and fiber angle with a gradient-based optimization algorithm. Adjoint design sensitivities are used to efficiently compute the design gradients. Various topology optimizations are performed using the MBB beam to illustrate our computational approach. Results show that once the modulus ratio exceeds about two, little difference is seen in the optimal topologies of the beam structure, and that the minimum compliance decreases with increase modulus ratio, as expected. The results also indicate that the optimal fiber angle generally aligns with the axis of truss members that form which has been seen by other researchers. A method is also presented for obtaining print path information from CFAO results. The resulting design are printed and tested and show that printed CFAO structures exhibit a higher stiffness than structures optimized for density alone. In summary, the CFAO method presented here is shown to provide optimal topologies and fiber angle for planar structures produced with carbon fiber-reinforced FFF structures.

Future work will extend the method given here to included structures with multiple loading conditions and three-dimensional design domains. The results appearing in this paper that include planar structures having a single load set is shown to produce fiber angles that mostly align with truss-like members that form during the topology optimization. Multiple load sets would likely yield quite different results, and may require that special attention be given to the element fiber angle, and how each element's angle varies with respect to its neighbor. It will be interesting to see if a fiber angle filtering method is required to obtain a printable solution. The extension of this approach to three-dimensions is also of interest where the added complexity will result from having non-planar design domains. Again, the continuity of fiber angle will be important here as well. The successful extension of this methodology to three dimensions is expected to make it possible to significantly impact FFF structural design.

| MBB Sample                 | Average (N/m)      | Standard Deviation (N/m) | Coefficient of Variation |
|----------------------------|--------------------|--------------------------|--------------------------|
| horizontal bead<br>[20,21] | $2.90 \times 10^5$ | $0.12 \times 10^5$       | 0.042                    |
| vertical bead<br>[20,21]   | $2.51 \times 10^5$ | $0.052 \times 10^5$      | 0.021                    |
| CFAO                       | $3.26 \times 10^5$ | $0.015 \times 10^5$      | 0.0047                   |

Table 2: Measured stiffness (average of 3 samples each) of printed CFAO optimized beams with other horizontal ( $\theta_e = 0$ ) and vertical ( $\theta_e = 90^\circ$ ) beams (cf. [20,21]) included for comparison

## Acknowledgements

The authors would like to thank the Dr. David Jack and the SIC'EM group at Baylor University for their collaboration and assistance, as well as the Baylor University Society of Plastics Engineers for their support.

## References

- [1] A. Bellini and G. Selcuk, "Mechanical characterization of parts fabricated using fused deposition modeling," *Rapid Prototyp. J.*, vol. 9, no. 4, pp. 252–264, 2003.
- [2] M. L. Shofner, K. Lozano, F. J. Rodríguez-Macías, and E. V. Barrera, "Nanofiber-reinforced polymers prepared by fused deposition modeling," *J. Appl. Polym. Sci.*, vol. 89, no. 11, pp. 3081–3090, Sep. 2003.
- [3] W. Zhong, F. Li, Z. Zhang, L. Song, and Z. Li, "Short fiber reinforced composites for fused deposition modeling," *Mater. Sci. Eng. A*, vol. 301, pp. 125–30, 2001.
- [4] F. Ning, W. Cong, J. Wei, S. Wang, and M. Z. Zhang, "Additive Manufacturing of CFRP Composites using Fused Deposition Modeling: Effects of Carbon Fiber Content and Length," in *Proceedings of the ASME 2015 International Manufacturing Science and Engineering Conference*, Charlotte, NC, 2015.
- [5] H. de A. Almeida and P. J. da Silva Bártolo, "Virtual topological optimisation of scaffolds for rapid prototyping," *Med. Eng. Phys.*, vol. 32, no. 7, pp. 775–782, Sep. 2010.
- [6] N. P. Fey, B. J. South, C. C. Seepersad, and R. R. Neptune, "Topology Optimization and Freeform Fabrication Framework for Developing Prosthetic Feet," presented at the Solid Freeform Fabrication Symposium, University of Texas at Austin, 2009.
- [7] M. P. Bendsoe, "Generating optimal topologies in structural design using a homogenization method," *Comput. Methods Appl. Mech. Eng.*, vol. 71, no. 2, pp. 197–224, 1988.
- [8] H. P. Jia, C. D. Ling, G. P. Li, R. Q. Mu, and C. B. Jiang, "Topology Optimization of Orthotropic Material Structure," *Mater. Sci. Forum*, vol. 575–578, pp. 978–989, Apr. 2008.
- [9] M. P. Bendsøe, "Optimal shape design as a material distribution problem," *Struct. Optim.*, vol. 1, no. 4, pp. 193–202, Dec. 1989.
- [10] R. J. Yang and C. H. Chuang, "Optimal topology design using linear programming," *Comput. Struct.*, vol. 52, no. 2, pp. 265–275, Jul. 1994.
- [11] J. M. Taboas, R. D. Maddox, P. H. Krebsbach, and S. J. Hollister, "Indirect solid free form fabrication of local and global porous, biomimetic and composite 3D polymer-ceramic scaffolds," *Biomaterials*, vol. 24, no. 1, pp. 181–194, Jan. 2003.
- [12] V. Sundararajan, "Topology Optimization for Additive Manufacturing of Customized Meso-Structures using Homogenization and Parametric Smoothing Functions," MS, University of Texas at Austin, 2010.
- [13] P. Zhang, J. Toman, Y. Yu, E. Biyikli, M. Kirca, M. Chmielus, and A. C. To, "Efficient Design-Optimization of Variable-Density Hexagonal Cellular Structure by Additive Manufacturing: Theory and Validation," *J. Manuf. Sci. Eng.*, vol. 137, no. 2, pp. 021004–021004, Apr. 2015.
- [14] J. Alamo and F. da Silva, "Adapting the SIMP Model for Topology Optimization of Biomechanical Structures," presented at the 12th Pan-American Congress of Applied Mechanics - PACAM XII, 2012.
- [15] O. Sigmund, "A 99 line topology optimization code written in Matlab," *Struct. Multidiscip. Optim.*, vol. 21, no. 2, pp. 120–127, Feb. 2014.

- [16] O. Sigmund and J. Petersson, "Numerical instabilities in topology optimization: A survey on procedures dealing with checkerboards, mesh-dependencies and local minima," *Struct. Optim.*, vol. 16, no. 1, pp. 68–75, Aug. 1998.
- [17] A. Michell, "The limits of economy of material in frame structures," *Philos. Mag.*, vol. 8, no. 47, pp. 589–597, 1904.
- [18] E. Andreassen, A. Clausen, M. Schevenels, B. S. Lazarov, and O. Sigmund, "Efficient topology optimization in MATLAB using 88 lines of code," *Struct. Multidiscip. Optim.*, vol. 43, no. 1, pp. 1–16, Nov. 2010.
- [19] K. Liu, "Top3dSTL\_v3," *Top3d: An Efficient 3D Topology Optimization Program*, Apr-2015. [Online]. Available: <https://top3dapp.com/download-archive/>. [Accessed: 04-Aug-2015].
- [20] Hoglund, R.M. and Smith, D.E., "Non-Isotropic Material Distribution Topology Optimization for Fused Deposition Modeling Products," in *Proceeding of the 2015 Solid Freeform Fabrication Symposium*, Austin, TX, pg. 888, August, 2015.
- [21] Hoglund, R.M., *An Anisotropic Topology Optimization Method for Carbon Fiber-Reinforced Fused Filament Fabrication*, MS Thesis, Baylor University, 2016.